HHS Public Access

Author manuscript

J Neurovirol. Author manuscript; available in PMC 2017 October 27.

Published in final edited form as:

J Neurovirol. 2017 October ; 23(5): 657–670. doi:10.1007/s13365-017-0545-9.

Regulation of T-type Ca^{2+} channel expression by herpes simplex virus-1 infection in sensory-like ND7 cells

Qiaojuan Zhang[1], **Shao-Chung Hsia**[1], and **Miguel Martin-Caraballo**[1]

[1]Department of Pharmaceutical Sciences, School of Pharmacy, University of Maryland Eastern Shore, Princess Anne, MD 21853, USA

Abstract

Infection of sensory neurons by herpes simplex virus (HSV)-1 disrupts electrical excitability, altering pain sensory transmission. Because of their low threshold for activation, functional expression of T-type Ca^{2+} channels regulates various cell functions, including neuronal excitability and neuronal communication. In this study, we have tested the effect of HSV-1 infection on the functional expression of T-type Ca^{2+} channels in differentiated ND7-23 sensory-like neurons. Voltage-gated Ca^{2+} currents were measured using whole cell patch clamp recordings in differentiated ND7-23 neurons under various culture conditions. Differentiation of ND7-23 cells evokes a significant increase in T-type Ca^{2+} current densities. Increased T-type Ca^{2+} channel expression promotes the morphological differentiation of ND7-23 cells and triggers a rebound depolarization. HSV-1 infection of differentiated ND7-23 cells causes a significant loss of T-type Ca^{2+} channels from the membrane. HSV-1 evoked reduction in the functional expression of T-type Ca^{2+} channels is mediated by several factors, including decreased expression of $Ca_V3.2$ T-type Ca^{2+} channel subunits and disruption of endocytic transport. Decreased functional expression of T-type Ca^{2+} channels by HSV-1 infection requires protein synthesis and viral replication, but occurs independently of Egr-1 expression. These findings suggest that infection of neuron-like cells by HSV-1 causes a significant disruption in the expression of T-type Ca^{2+} channels, which can results in morphological and functional changes in electrical excitability.

Keywords

Sensory neuron; Calcium channel; Pain; Electrical excitability

Introduction

Herpes simplex virus type 1 (HSV-1) is a neurotropic pathogen associated with painful oral lesions and severe ocular and brain complications. Following infection of sensory neurons, HSV-1 can establish latency and later undergo reactivation in response to various factors,

Correspondence to: Miguel Martin-Caraballo.

Author contributions QJZ: designed/performed experiments, SCH: reviewed/edited the manuscript, MMC: designed/performed experiments/ wrote the manuscript. All authors read and approved the final manuscript.

Compliance with ethical standards

Conflict of interest The authors declare that they have no conflicts of interest.

including stress, cold temperature, and skin trauma, resulting in the development of cold sores (Antoine et al., 2013). Viral infection depends on several critical steps including attachment to specific receptors on the host cell membrane and entry and replication of viral genes (Agelidis et al., 2015). HSV-1 entry can occur either by direct fusion of the viral envelope with the host cell membrane or by an endocytic mechanism.

Changes in intracellular Ca^{2+} concentration regulate a variety of cellular processes including viral entry (Cheshenko et al., 2007; Zhou et al., 2009). In neuronal cells, the intracellular Ca^{2+} concentration is tightly regulated by Ca^{2+} entry via voltage- and/or ligand-gated channels, release from intracellular Ca^{2+} stores, and cellular buffering. Although HSV-1 promotes Ca^{2+} release from intracellular stores, it is unclear how viral infection alters the function of voltage-gated Ca^{2+} channels (VGCC) in neuronal cells. Based on their biophysical and pharmacological properties, VGCC are broadly divided into low voltage- and high voltage-activated Ca^{2+} channels (LVA and HVA, respectively; reviewed by Catterall, 1998). LVA (or T-type) Ca^{2+} channels generate transient currents at relatively hyperpolarized membrane potentials. Expression of T-type Ca^{2+} channels on the membrane is regulated by a variety of factors, including signaling molecules and the redox state (reviewed by Iftinca and Zamponi, 2009).

Functional expression of T-type Ca^{2+} channels regulates neuronal excitability, which plays a significant role in the transmission of pain information (Todorovic and Jevtovic-Todorovic, 2011). Primary and secondary HSV-1 infections often cause alterations in pain sensory transmission with both diminished and enhanced pain signaling having being reported (Andoh et al., 1995). The role of HSV-1 infection in regulating T-type Ca^{2+} channel expression has not been characterized. In this work, we have tested the effect of HSV-1 viral infection on T-type Ca^{2+} channel expression in sensory neuron-like ND7-23 cells. ND7-23 cells were generated by the fusion of mouse neuroblastoma N18Tg2 with rat DRG cells, thus providing a homogenous cell population with sensory neuron-like properties (Wood et al., 1990).

Methods

Culture, differentiation, and infection of ND7-23 cells

ND7-23 cells were obtained from Sigma-Aldrich (St. Louis, MO). Undifferentiated cells were grown in DMEM-high glucose growth media supplemented with 10% fetal bovine serum, 50 U/ml penicillin and 50 μg/ml streptomycin at 37 °C with a 5% CO_2/95% air humidified atmosphere, as previously described by Wood et al. (1990). Cell differentiation was induced by exposing the cells to differentiation media, consisting of DMEM/F12, supplemented with 0.5% fetal bovine serum and db-cAMP (1 mM), or NGF (50 ng/mL, Sigma-Aldrich) or db-cAMP+NGF as previously described (Wood et al., 1990; Storey et al., 2002). ND7-23 cells were maintained in differentiation media for 4–10 days. Cells were grown either in 6-well plates or on poly-D-lysine-coated glass coverslips (for whole cell recordings).

Unless otherwise specified, viral infections were performed with a HSV-1 strain 17Syn+-GFP virus (A1 strain, Foster et al., 1998). We also assessed the effect of an HSV-1 viral

construct expressing early growth response (Egr)-1 (A7 strain, Bedadala et al., 2014). Both HSV-1 strains also express GFP, which facilitates the identification of infected cells. Cell cultures were exposed to HSV-1 for 1 h in a cell culture incubator, as previously described (Bedadala et al., 2011). After this time period, unbound viral particles were washed out and fresh media supplemented with different drug combinations was applied.

Morphometric analysis

Images of cultured ND7-23 cells were obtained with a Nikon Eclipse Ti microscope with a 20× inverted objective and a Photometrics Coolsnap EZ cooled camera. The following parameters were assessed to determine changes in cell morphology: total neurite-like length and number of primary neurite-like processes emanating per the cell body. These parameters were measured using the Nikon NIS-Elements imaging software.

Western blot analysis

Immunoblot analysis was conducted using a specific antibody against the $Ca_v3.2$ subunit (Cat.# sc-25691, Santa Cruz, Dallas, TX) or Egr-1 (Cat.# sc-20690, Santa Cruz, Dallas, TX). Cell lysates were combined with Bolt LDS sample buffer (ThermoFisher, Grand Island, NY), supplemented with reducing agent and boiled for 10 min. Proteins were separated on SDS-PAGE 8% gels (Bolt Bis-Tris Plus Gels, ThermoFisher, Grand Island, NY). Proteins were transferred to nitrocellulose membranes using the Invitrogen iBlot system, followed by incubation in SuperBlock blocking buffer for 45 min (ThermoFisher, Grand Island, NY) before overnight incubation with rabbit anti-$Ca_v3.2$ (1:500) or rabbit anti-Egr-1 (1:1000). Blots were analyzed using anti-rabbit-secondary antibodies conjugated to horseradish peroxidase and a chemiluminescent substrate (SuperSignal West Pico, ThermoFisher, Grand Island, NY). To control for equal loading of protein in each sample, membranes were stripped in stripping buffer (Restore Plus stripping buffer, ThermoFisher, Grand Island, NY) for 30 min at room temperature (22–24 °C) and reprobed with a tubulin-specific antibody (at 1:2000 dilution, Cat.# 05-829, Upstate) followed by incubation with the corresponding secondary antibody and immunodetection. Changes in $Ca_v3.2$ protein expression were determined by densitometry analysis using the Image Lab software (Bio-Rad, Hercules, CA).

Electrophysiology

ND7-23 cells were visualized using a Nikon Eclipse Ti inverted microscope (Nashua, NH, USA) equipped with Hoffman optics and epifluorescence filters. Infected cells were identified by the expression of GFP. Recordings were performed at room temperature (22–24 °C). Recording electrodes were made from thin wall borosilicate glass (3–4 MΩ) and filled with a solution consisting of (in mM) CsCl (120), $MgCl_2$ (2), HEPES-KOH (10), EGTA (10), ATP (1), and GTP (0.1), pH 7.4 with CsOH. Normal external saline for measurements of Ca^{2+} currents contained (in mM): tetraethylammonium chloride (TEACl, 145), $CaCl_2$ (10), $MgCl_2$ (1), and HEPES (10), pH 7.4 adjusted with CsOH. Normal external saline for measurements of Na^+ currents contained (in mM): NaCl (145), KCl (5.4), $MgCl_2$ (0.8), $CaCl_2$ (5.4), glucose (5), and HEPES (13), pH 7.4 adjusted with NaOH. Ca^{2+} currents were generated by applying either a 750 ms-voltage ramp from −110 to +80 mV or a 200 ms-depolarizing step to various potentials. To isolate the T-type Ca^{2+} currents, a series of

200 ms-depolarizing step to various potentials was applied from either a holding potential of −110 or −40 mV. Net T-type Ca^{2+} currents were obtained by digital subtraction ($I_{-110} - I_{-40}$). The current-voltage relationship was obtained as previously described by Pachuau and Martin-Caraballo (2007) using the net T-type Ca^{2+} current traces. Na^{+} currents were generated by applying a 100-ms depolarizing step to various potentials from a holding potential of −100 mV. Voltage commands, data acquisition, and analysis were performed with a MULTICLAMP 700A amplifier and the PCLAMP software (Axon Instruments, Foster City, CA). Pipette offset, whole cell capacitance, and series resistance (usually <10 MΩ) were compensated automatically with the MultiClamp 700B Commander. Sampling rates were between 5 and 10 kHz. For quantitative analysis, cell size was normalized by dividing current amplitudes by cell capacitance, determined by integration of the transient current evoked by a 10-mV voltage step from a holding potential of −60 mV (Pachuau and Martin-Caraballo, 2007).

The activation (τ_{act}) and inactivation (τ_{inact}) time constants were obtained by fitting the rising or decay portion of the transient currents with one exponential function in the form $I(t) = A\exp(-t/\tau)$, where A is peak current and τ is the time constant. The membrane potential that elicited maximal channel opening was determined from the current ramp.

Membrane voltage responses were recorded in the current clamp configuration. Changes in membrane potential were generated by applying either depolarizing or hyperpolarizing currents from a holding potential of ~−60 mV. Current commands, data acquisition, and analysis were performed with a MULTICLAMP 700A amplifier and PCLAMP software. All data values are presented as mean ± SEM. Statistical analyses consisted of Student's unpaired t test when single comparisons were made and one-way ANOVA followed by post hoc analysis using Tukey's honest significant difference test for unequal n for the more typical experimental designs that entailed comparisons between multiple groups (STATISTICA software, Tulsa, OK). Throughout, $p < 0.05$ was regarded as significant. In every experiment, data was collected from a minimum of two platings (i.e., from multiple cultures).

Plaque assay

The plaque assay was performed as previously described (Hsia et al., 2013). Briefly, cells were plated in 12-well plates and seeded at a concentration of 1.6×10^5 cells/mL overnight. The supernatant of infected cells was collected and serially diluted before being added to cultured cells. After 48 hpi, wells were washed with PBS, fixed with methanol, and stained with crystal violet prior to counting plaque formation.

Quantitative PCR

Quantification of thymidine kinase (TK) expression was performed as previously described (Figliozzi et al., 2014). Briefly, genomic DNA was isolated using the GeneElute™ Mammalian Genomic DNA Miniprep Kit (Sigma-Aldrich). SYBR green supermix (Bio-Rad) was used to perform the qPCR reactions on triplicate samples. The set of primers used to amplify the TK gene expression was as follows: forward, 5′-ATG GCT TCG TAC CCC TGC CAT-3′, reverse, 5′-GGT ATC GCG CGG CCG GGT A-3′. qPCR reactions were

carried out at 98 °C for 3 min, 98 °C for 10 s, followed by 58 °C for 30 s (39 cycles), 65 °C for 15 s, and 72 °C for 15 s. TK expression was normalized to that of peptidylpropyl isomerase A (PPIA, forward, 5′-AGC ATA CGG GTC CTG GCA TCT-3′, reverse, 5′-CAT GCT TGC CAT CCA ACC ACT CA-3′).

Reagents

Acyclovir, brefeldin-A, chloroquine, cycloheximide, and lactacystin were purchased from Sigma-Aldrich. Cell culture reagents were obtained from Invitrogen.

Results

ND7-23 cells were cultured for 4–10 days in growth media or differentiation media, supplemented with NGF, db-cAMP or NGF+db-cAMP. Ca^{2+} currents were isolated by substitution of Na^+ ions with external tetraethylammonium (TEA) and by including Cs^+ ions in the pipette solution to block outward K^+ currents (see the “Methods” section). To enhance the amplitude of Ca^{2+} currents, we included 10 mM $BaCl_2$ in the external solution. An example of the Ca^{2+} current generated in differentiated ND7-23 cells is represented in Fig. 1 (A). Maximal LVA (T-type) Ca^{2+} currents were generated by voltage steps from a holding potential of −110 mV, whereas HVA Ca^{2+} currents were evoked by voltage steps from a holding potential of −40 mV (Fig. 1 (Aa) and (Ab), respectively). Initially, we characterized the expression of LVA and HVA Ca^{2+} currents in ND7-23 cell under different culture conditions. Both currents were observed in differentiated ND7-23 under different culture conditions. However, T-type Ca^{2+} currents were detected in the majority of recorded neurons, whereas HVA currents were only observed in ~40% of all recorded neurons. Application of voltage steps from a holding potential of −110 mV revealed a transient Ca^{2+} current that was eliminated following application of voltage steps from a holding potential of −40 mV (Fig. 1 (Aa), (Ab)), indicating that activation of the transient component was voltage-sensitive. Subtraction of current traces generated from a holding potential of −110 and −40 mV was used to quantify the total T-type Ca^{2+} currents expressed in ND7-23 cells (Fig. 1 (Aa–b)). To differentiate between LVA and HVA currents, we also recorded Ca^{2+} currents evoked by a 750-ms depolarizing voltage ramp from a holding potential of −100 mV (Fig. 1 (Ba)). Recording of Ca^{2+} currents following application of the voltage ramp revealed the presence of an early and a late components, generated by activation of LVA and HVA Ca^{2+} channels, respectively (Dey et al., 2011). The LVA component in the voltage ramp was sensitive to inhibition by low concentrations of $NiCl_2$ (100 μM) or NNC 55-0396 (5 μM) (Fig. 1 (Bb)). Whole cell Ca^{2+} currents were normalized to cell size by dividing current amplitudes by cell capacitance in order to compensate for changes in cell size that may occur under different culture and treatment conditions (Pachuau and Martin-Caraballo, 2007). The resulting current densities were used to assess changes in the functional expression of T-type Ca^{2+} channels in the membrane. There were no significant changes in the cell capacitance of ND7-23 cells cultured in the presence of growth or differentiation media for up to 10 d (Fig. 1 (C)). However, T-type Ca^{2+} current density was significantly lower in ND7-23 cells cultured in growth media compared to differentiated cells (Fig. 1 (D)). Since Ca^{2+} channel expression may be altered by cAMP and trophic factors (Garber et al., 1989; Kim et al., 2006; Woodall et al., 2008), we compared the effect of these factors on

T-type Ca^{2+} currents. Culture of ND7-23 cells in differentiation media with or without NGF resulted in equivalent levels of T-type Ca^{2+} current densities (Fig. 1 (D)). T-type Ca^{2+} current densities were significantly higher in ND7-23 cells cultured in differentiation media supplemented with db-cAMP (Fig. 1 (D)). Culture of ND7-23 cells in differentiation media supplemented with NGF or db-cAMP did not alter the activation (τ_{act}) and inactivation (τ_{inact}) time constants of T-type Ca^{2+} channels compared with cells cultured in differentiation media alone [τ_{act}, DM = 3.3 ± 0.4, DM + NGF = 3.1 ± 0.1, DM + db-cAMP = 2.4 ± 0.2 ms ($n = 11$, $p > 0.5$); τ_{inact}, DM = 19.3 ± 1.4, DM + NGF = 19.4 ± 1.0, DM + db-cAMP = 17.3 ± 2.1 ms ($n = 11$, $p > 0.5$). We should point out, however, that culture of ND7-23 cells in differentiation media supplemented with db-cAMP caused a leftward shift in the activation voltage needed to reach maximal channel opening as assessed from the voltage ramp (DM = −27.5 ± 2.6, DM + NGF = −33.4 ± 1.9, DM + db-cAMP = −39.8 ± 2.0* mV ($n = 11$, *$p < 0.5$ vs. DM).

Undifferentiated ND7-23 cells presented a round morphology with no neurite outgrowth (not shown). Culture of ND7-23 cells in differentiation media resulted in the development of several neurite-like processes (Fig. 2a). The growth of dendritic processes was sensitive to inhibition of T-type Ca^{2+} channel function (Fig. 2b–e). Thus, treatment of differentiated ND7-23 cells with low concentration of $NiCl_2$ (100 μM) or NNC 55-0396 (5 μM) resulted in a significant reduction in the dendritic length and the number of processes/cell compared with non-treated controls (Fig. 2d–e).

The effect of HSV-1 infection on T-type Ca^{2+} current densities was studied in cells infected for 3–48 h. Infected cells were identified by the expression of GFP (Fig. 3 (A, B)). Phase and GFP fluorescence images of differentiated ND7-23 cells infected with HSV-1 indicate a significant level of infection as assessed by GFP expression (Fig. 3 (Ba and Bb)). In cases where gene expression was blocked (see below), a higher moi was used to infect the majority of cells. Infection of differentiated ND7-23 cells for 24–48 h caused a significant reduction in the T-type Ca^{2+} current densities without any significant change in cell capacitance (Fig. 3 (C, D)). Similar results were also obtained in ND7-23 culture in differentiation media, supplemented with db-cAMP, suggesting that viral infection causes a significant reduction in T-type Ca^{2+} channel expression independently of cAMP activation (Fig. 3 (C, D)). HSV-1 infection did not alter the current-voltage relationship of T-type Ca^{2+} channels (Fig. 3 (E)). HSV-1 infection had no effect on the properties of the T-type Ca^{2+} currents. For example, there were no changes in the activation time (τ_{act}, control = 2.6 ± 0.3 vs. HSV = 3.2 ± 0.3 ms, $n = 7$, $p > 0.5$), inactivation time (τ_{inact}, control = 22.4 ± 2.7 vs. HSV = 32.4 ± 8.5 ms, $n = 7$, $p > 0.5$) or activation voltage needed to reach maximal channel opening (control = −32.7 ± 2.6 vs. HSV = −31.1 ± 1.9 mV, $n = 7$, $p > 0.5$). However, HSV-1 infection of differentiated ND7-23 cells causes a reduction in the protein expression of the T-type Ca^{2+} channel subunit $Ca_v3.2$ as assessed by immunoblot analysis (Fig. 3 (F)).

The effect of viral infection on T-type Ca^{2+} channel expression requires some time to develop since exposure to HSV-1 for 3 h did not have any significant effect on T-type Ca^{2+} currents or cell capacitance (Fig. 4a, b). Since HSV-1 viral infection induces expression of early growth response-1 (Egr-1) proteins (Bedadala et al., 2011), which can consequently alter the expression of T-type Ca^{2+} channels (van Loo et al., 2012), we assessed the effect of

a HSV-1 viral construct overexpressing the Egr-1 gene (HSV-1 viral A7 strain, Bedadala et al., 2014). Immunoblot analysis reveals that infection of differentiated ND7-23 cells with the HSV-1 A7 viral strain caused a significant increase in Egr-1 protein expression, compared to Egr-1 expression in control or following infection with the HSV-1 A1 viral strain (Fig. 5a). Infection of differentiated ND7-23 cells with the Egr-inducing HSV-1 A7 viral strain caused a significant reduction in T-type Ca^{2+} channel expression without altering cell capacitance (Fig. 5b, c).

A reduction in the functional expression of T-type Ca^{2+} channels caused by HSV-1 infection of ND7-23 cells can be the result of several factors, including increased internalization/degradation of channels already present in the membrane or reduced trafficking of new channels to the membrane. HSV-1 evoked changes in T-type Ca^{2+} channel expression can also be affected by changes in protein synthesis and viral replication. To determine what factors regulate the functional expression of T-type Ca^{2+} channels in differentiated ND7-23 cells following infection by HSV-1, we followed a pharmacological approach. First, we assessed whether the effect of HSV-1 infection on T-type Ca^{2+} channel expression was affected by inhibiting protein synthesis or viral replication. Protein synthesis was inhibited with cycloheximide (CHX, 50 μg/mL), whereas viral replication was blocked with acyclovir (ACV, 150 μM). Previous work indicates that these concentrations of cycloheximide and acyclovir are effective in blocking protein synthesis and viral replication, respectively (Weinheimer and McKnight, 1987; Hsia et al., 2013). Second, we tested whether the effect of HSV-1 infection on T-type Ca^{2+} channel expression was affected by disputing the trans-Golgi transport with brefeldin-A (BFA, 1 μg/mL). Brefeldin-A (1 μg/mL) blocks protein trafficking between the Golgi and the membrane (Dey et al., 2011). Third, we tested the effect of chloroquine (CQ, 100 μM) or lactacystin (5 μM) to study the effect of endosomal internalization on T-type Ca^{2+} channel expression following HSV-1 infection. Chloroquine blocks the acidification of endosomal particles, inhibiting clathrin-dependent membrane internalization and endosomal trafficking (Daniels and Amara, 1999). Lactacystin (LC) blocks proteasome function and the degradation of ubiquitinated proteins (Shah and Di Napoli, 2007; Delboy et al., 2008). To allow for viral binding and internalization, cell cultures were exposed to HSV-1 for 1 h before exposure to individual drugs. In our first set of experiments, we investigated the effect of cyclohexamide, acyclovir, brefeldin-A, chloroquine, and lactacystin on cell capacitance and T-type Ca^{2+} channel expression in differentiated ND7-23 cells not infected with HSV-1. Whole cell recordings revealed that only acyclovir and brefeldin-A caused a significant reduction in cell capacitance compared to control cells (Fig. 6a). None of the drug treatments used on differentiated ND7-23 cells had any effect on T-type Ca^{2+} current densities (Fig. 6b), indicating that these treatments had no effect on channels already present in the membrane.

In differentiated ND7-23 cells, overnight HSV-1 infection caused a significant reduction in T-type Ca^{2+} current density compared with control cells, without altering cell capacitance (Fig. 6c, d). Inhibition of protein synthesis and viral replication with cycloheximide and acyclovir after 1 h infection with HSV-1 reversed the inhibitory effect of the virus on T-type Ca^{2+} current densities (Fig. 6d). Thus, cycloheximide and acyclovir caused a significant increase in T-type Ca^{2+} current densities in ND7-23 cells infected with HSV-1, compared with cells that were expose to the virus alone (Fig. 6d). Only cycloheximide treatment of

HSV-1 infected ND7-23 cells increases cell capacitance, whereas acyclovir had no statistically significant effect on cell size (Fig. 6c). These findings suggest that inhibition of protein synthesis and viral replication regulate the reduction in T-type Ca^{2+} channel expression evoked by HSV-1 infection in ND7-23 cells. Inhibition of trans-Golgi trafficking also reverted the inhibitory effect of HSV-1 infection on T-type Ca^{2+} current density without having any effect on cell capacitance (Fig. 6d, c). Inhibition of clathrin-dependent membrane internalization and endosomal trafficking also evoked a significant increase in T-type Ca^{2+} current density in HSV-1-infected cells compared to cells exposed to the virus alone without any further change in cell capacitance (Fig. 6d, c). On the contrary, lactacystin had no effect on abolishing the inhibitory effect of HSV-1 infection on T-type Ca^{2+} current density (Fig. 6d). However, lactacystin causes a significant increase in cell capacitance (Fig. 6c).

To investigate the effect of these pharmacological treatments on viral replication, we performed qPCR analysis to measure viral genome copy number using primer pairs against the thymidine kinase (TK) gene and plaque assay analysis of viral release. The qPCR signal is associated with increased viral replication following HSV-1 infection (Hsia et al., 2010). The plaque assay assesses the release of viral particles and their infectious potential. As shown in Fig. 7a, b, treatment of differentiated ND7-23 cells with cyclohexamide and acyclovir caused a significant reduction in TK gene expression and the complete elimination of plaque formation following HSV-1 infection. Similarly, treatment of differentiated ND7-23 cells with chloroquine, brefeldin-A, and lactacystin caused a significant decrease in TK signal and plaque formation following HSV-1 infection.

The expression of T-type Ca^{2+} channels results in the presence of a rebound depolarization following the injection of hyperpolarizing currents (Martin-Caraballo and Greer, 2001). Rebound depolarization is triggered by the removal of the voltage-dependent inactivation of T-type Ca^{2+} channels and increases neuronal excitability (Martin-Caraballo and Greer, 2001). To assess whether expression of T-type Ca^{2+} channels in differentiated ND7-23 cells triggers rebound depolarization, we performed current clamp recordings to detect changes in membrane potential following injection of hyperpolarizing current (Fig. 8). To enhance the expression of rebound depolarization, membrane voltage responses to injection of hyperpolarizing currents were recorded in the presence of an external solution, supplemented with 10 mM $BaCl_2$ and containing TEACl to block voltage-activated Na^+ channels, and a pipette solution containing CsCl to block voltage-activated K^+ channels. Our results demonstrate that in non-infected cells, injection of hyperpolarizing currents results in a rebound depolarization that is eliminated following the infection of differentiated ND7-23 cells with HSV-1 (Fig. 8a, b). Because of the recording conditions, no Na^+-dependent action potentials were evident as assessed by the membrane responses generated by injections of depolarizing currents (Fig. 8b, c).

Does HSV-1 infection of differentiated ND7-23 cells also have an effect on the expression of voltage-activated Na^+ currents? To investigate this possibility, we recorded the Na^+ currents generated by a series of voltage steps from a holding potential of −100 mV. In differentiated ND7-23 cells, Na^+ currents peaked at a depolarizing membrane potential of +20 mV (Fig. 9a). The current-voltage relationship shows a significant reduction in the amplitude of Na^+ currents following infection of differentiated ND7-23 cells with HSV-1 (Fig. 9a). There were

no significant differences in the cell capacitance before or after HSV-1 infection (Fig. 9b). However, HSV-1 infection caused a significant reduction in the density of Na^+ currents generated by a voltage step to +20 mV (Fig. 9c).

Discussion

In this study, we have examined the effect of HSV-1 infection on the functional expression of T-type Ca^{2+} channels in sensory-like ND7-23 cells. Three main conclusions can be drawn from these experiments. First, functional expression of T-type Ca^{2+} channels on the membrane of differentiated ND7-23 cells is significantly reduced by HSV-1 infection. Second, HSV-1 evoked reduction of T-type Ca^{2+} channel expression depends on viral replication and protein synthesis. Third, HSV-1 evoked reduction of T-type Ca^{2+} channel expression involves decreased expression of the $Ca_v3.2$ channel subunit and endosomal degradation of T-type Ca^{2+} channels already present in the membrane.

Our present results demonstrate that infection of differentiated ND7-23 cells with HSV-1 cause a significant reduction in the functional expression of T-type Ca^{2+} channels already present in the membrane. The inhibitory effect of HSV-1 infection on T-type Ca^{2+} channel expression requires more than 3 h to develop and results in an ~80% reduction of functional channels 24–48 h post-infection. Previous studies have shown that HSV-1 infection alters the electrophysiological properties of infected neurons, which could have a significant effect on electrical excitability and transmission of sensory information (Oakes et al., 1981; Storey et al., 2002). In dorsal root ganglion (DRG) cells, HSV-1 infection causes a significant reduction in the membrane expression of voltage-activated Na^+ channels due primarily to increased internalization of channels already present in the membrane (Storey et al., 2002). Our present results also confirm that infection of differentiated ND7-23 cells with HSV-1 also causes a significant reduction in the Na^+ current densities. However, infection of ND7 cells with the varicella-zoster herpes virus that causes chickenpox results in a significant increase in Na^+ current densities (Kennedy et al., 2013). Thus, herpes viral infection can have various effects on ion channel expression. In this work, we recorded whole cell Ca^{2+} currents in differentiated cells with dendritic processes and clear HSV-1 infection as indicated by GFP expression. Our findings show that HSV-1 infection of differentiated ND7-23 cells results in a significant reduction in the functional expression of T-type Ca^{2+} channels. However, others have found that HSV-1 infection of DRG neurons has no effect on the functional expression of voltage-activated Ca^{2+} channels, including T-type Ca^{2+} channels (Storey et al., 2002). This difference could be explained by the nature of recorded cells or by cell-specific differences. First, our recordings were performed in GFP-positive ND7-23 cells, indicating a significant level of viral replication. Recordings of T-type Ca^{2+} currents in DRG cells were not correlated with the level of viral replication (Storey et al., 2002). Second, cell-specific differences related to changes in signaling molecules could underlie the lack of effect of HSV infection on the expression of T-type Ca^{2+} channels in DRG neurons compared with differentiated ND7-23 cells. Functional expression of T-type Ca^{2+} channels is regulated by a variety of signaling mechanisms, including redox state and phosphorylation by various kinases (Chemin et al., 2006). DRG cells consist of a heterogeneous population of neurons with distinct electrophysiological properties and various functional roles, including the transmission of sensory signals for pain, temperature,

and touch (Scott and Edwards, 1980; MeLean et al., 1988). On the contrary, ND7-23 cells are derived from a fusion clone of rat DRG cells with a mouse neuroblastoma cell line, generating a more homogenous population of sensory-like neurons (Wood et al., 1990). A transcriptome analysis of these neuronal populations indicates expression of common molecular markers such as RET (a marker for myelinated and unmyelinated neurons), tyrosine hydroxylase (TH), tyrosine receptor kinase A (TrkA), and transient receptor potential channel subunits (TRP) (Yin et al., 2016). However, there are noticeable differences in the expression of several ion channels and signalling molecules (Yin et al., 2016). Although HSV infection altered the functional expression of T-type Ca^{2+} channels in differentiated ND7-23 cells but not DRG neurons, it remains to be determined whether this regulatory mechanism interferes with channel expression in other major targets of HSV-1 infection such as trigeminal neurons.

Functional expression of T-type Ca^{2+} channels on the membrane is regulated by several factors, including synthesis of new channel proteins, trafficking of assembled channels from the Golgi to the membrane, and internalization/degradation of channel proteins. Differentiated ND7-23 cells express a significant quantity of functional T-type Ca^{2+} channels on the membrane as our whole cell recordings demonstrate. However, HSV-1 infection results in a significant reduction of functional T-type Ca^{2+} channels. Thus, the question arises as to the cellular mechanism(s) that alter T-type Ca^{2+} channel membrane expression following HSV-1 infection. Our present results demonstrate that following HSV-1 infection, there is a significant reduction in the expression of the $Ca_V3.2$ channel subunit, which could explain the reduction of functional channels by viral infection. Cycloheximide and acyclovir treatment of differentiated ND7-23 cells evoked a significant reduction in TK gene expression and resulted in complete elimination of plaque formation indicating a significant disruption in viral replication and the synthesis of new viral particles. It appears that viral replication and synthesis of viral proteins regulate the effect of HSV-1 infection on T-type Ca^{2+} channels in ND7-23 neurons. Thus, cycloheximide and acyclovir treatment of differentiated ND7-23 cells reversed the inhibitory effect of HSV-1 infection on functional T-type Ca^{2+} channels. Cycloheximide treatment alone did not have any effect on the functional expression of functional T-type Ca^{2+} channels, suggesting that synthesis and insertion of new channel proteins is not a critical factor regulating the number of channels over a 24 h period. Thus, our results indicate that viral replication and synthesis of new viral proteins interferes with the normal membrane expression of T-type Ca^{2+} channels. We should also mention that disruption of T-type Ca^{2+} channel expression by HSV-1 infection is not a simple matter of viral binding and entry into the host cells since recordings of whole cell Ca^{2+} channels 3 h post-infection did not result in any significant change in current amplitudes. HSV-1 viral infection results in the transcription of immediate early genes, which led to the expression of early and late viral proteins that are necessary for viral replication (Weinheimer and McKnight, 1987; Everett, 2000). As previously reported, cycloheximide blocks protein synthesis and viral replication (Preston and Nicholl, 1997). Thus, it appears that viral protein synthesis plays a role in regulating the overall expression of T-type Ca^{2+} channels on the membrane. Although viral protein synthesis regulates the effect of HSV-1 on T-type Ca^{2+} channel expression; this process is not affected by changes on Egr-1 expression. It has been previously reported that HSV-1 infection results in a

significant increase in Egr-1 protein, a transcriptional factor that promotes the upregulation of the $Ca_V3.2$ pore forming subunit of T-type Ca^{2+} channels (Bedadala et al., 2011; van Loo et al., 2012). However, infection of differentiated ND7-23 cells with an Egr-1 expressing HSV-1 viral construct (A7 strain) did not result in enhanced T-type Ca^{2+} channel expression on the membrane.

Our present results also indicate that disruption of trans-Golgi trafficking and endosome formation play a role in regulating the overall expression of T-type Ca^{2+} channels on the membrane. Thus, brefeldin-A and chloroquine treatment of differentiated ND7-23 cells reverses the inhibitory role of HSV-1 infection on T-type Ca^{2+} channel expression. Endosomal formation and post-Golgi trafficking are intrinsically coupled processes involved in the insertion and/or internalization of membrane proteins. Although viral penetration is not affected by the endosomal pathway (Wittels and Spear, 1991), the endocytic network and trans-Golgi trafficking regulate the assembly and secretion of viral particles from infected cells (Harley et al., 2001). Thus, our present results are consistent with the idea that HSV-1 promotes the internalization of T-type Ca^{2+} channels already present in the membrane. However, we cannot discard the possibility that the effect of brefeldin-A and chloroquine is mediated by a direct effect on viral replication. Thus, our present results indicate that both brefeldin-A and chloroquine also causes a significant reduction in TK gene expression and plaque formation.

Disruption of proteasome function and the degradation of ubiquitinated proteins did not alter the internalization of T-type Ca^{2+} channels already present in the membrane since lactacystin did not reverse the inhibitory effect of HSV-1 infection on channel expression. The proteasome pathway is involved in the proteolysis of ubiquitin-tagged intracellular proteins, which are destined for degradation. Although lactacystin did not reverse the inhibitory effect of HSV-1 infection on channel expression, it causes a significant reduction in TK gene expression and plaque formation, consistent with previous findings (Dai-Ju et al., 2006; Delboy et al., 2008). Thus, we expected lactacystin to reverse the effect of HSV-1 infection on channel expression. However, this was not the case, which could be related to other regulatory processes involving proteasome function, such as changes in cell surface area caused by HSV-1 infection. Consistent with this possibility, lactacystin generated a considerable increase in cell capacitance, which could have masked any increase in T-type Ca^{2+} channel expression.

Changes in the functional expression of voltage-activated ionic conductances following HSV-1 infection can disrupt neuronal excitability and sensory neurotransmission. T-type Ca^{2+} channels display low threshold activation at membrane potentials close to rest and fast inactivation. Activation of T-type Ca^{2+} channels plays a significant role in regulating neuronal excitability through changes in the action potential waveform and repetitive firing pattern (Umemiya and Berger, 1994; Martin-Caraballo and Greer, 2001). Our present results demonstrate that differentiated ND7-23 cells expressing T-type Ca^{2+} channels also generate a prominent rebound depolarization that can be eliminated following infection with HSV-1. Rebound depolarization enhances electrical excitability following the removal of voltage-dependent inactivation of T-type Ca^{2+} channels (Martin-Caraballo and Greer, 2001). Thus, disruption of T-type Ca^{2+} channel expression following HSV-1 infection can alter electrical

excitability and the ability of neurons to respond to sensory stimuli. Indeed, our present results demonstrate that HSV-1 evoked reduction in T-type Ca^{2+} channel expression prevents the development of rebound depolarization in infected neurons. Thus, disruption of T-type Ca^{2+} channel expression following HSV-1 infection may alter the ability of sensory neurons to transmit pain information. HSV-1 infection often results in significant alterations in pain sensory transmission with both diminished and enhanced pain signaling being reported (Krohel et al., 1976; Andoh et al., 1995; Takasaki et al., 2000). Functionally, reduced sensory neurotransmission due to lower expression of voltage-activated Na^{+} and Ca^{2+} currents during early viral infection could provide a stealth capability to further viral infection without detection by the host. Changes in ion channel expression can potentially enhance pain signaling at later stages of the viral infection as a result of cellular processes that remains to be investigated and that could be responsible for the development of post herpetic neuralgia.

Acknowledgments

This work was supported by funds provided by the UMES School of Pharmacy and grant R01NS081109 to SCH from NINDS/NIH. The content of this work is solely the responsibility of the authors and does not necessarily represent the official views of the NINDS/NIH. The funders had no role in study design, data collection and analysis, decision to publish, or preparation of the manuscript.

References

Agelidis AM, Shukla D. Cell entry mechanisms of HSV: what we have learned in recent years. Future Virol. 2015; 10(10):1145–1154. [PubMed: 27066105]

Andoh T, Shiraki K, Kurokawa M, et al. Paresthesia induced by cutaneous infection with herpes simplex virus in rats. Neurosci Lett. 1995; 190(2):101–104. [PubMed: 7644115]

Antoine TE, Park PJ, Shukla D. Glycoprotein targeted therapeutics: a new era of anti-herpes simplex virus-1 therapeutics. Rev Med Virol. 2013; 23(3):194–208. [PubMed: 23440920]

Bedadala G, Chen F, Figliozzi R, et al. Construction and characterization of recombinant HSV-1 expressing early growth response-1. ISRN Virol. 2014; 2014:1–7.

Bedadala GR, Palem JR, Graham L, et al. Lytic HSV-1 infection induces the multifunctional transcription factor early growth response-1 (EGR-1) in rabbit corneal cells. Virol J. 2011; 8:262. [PubMed: 21619646]

Chemin J, Traboulsie A, Lory P. Molecular pathways underlying the modulation of T-type calcium channels by neurotransmitters and hormones. Cell Calcium. 2006; 40(2):121–134. [PubMed: 16797700]

Cheshenko N, Liu W, Satlin LM, et al. Multiple receptor interactions trigger release of membrane and intracellular calcium stores critical for herpes simplex virus entry. Mol Biol Cell. 2007; 18(8):3119–3130. [PubMed: 17553929]

Catterall WA. Structure and function of neuronal Ca2+ channels and their role in neurotransmitter release. Cell Calcium. 1998; 24(5–6):307–323. [PubMed: 10091001]

Dai-Ju JQ, Li L, Johnson LA, et al. ICP27 interacts with the C-terminal domain of RNA polymerase II and facilitates its recruitment to herpes simplex virus 1 transcription sites, where it undergoes proteasomal degradation during infection. J Virol. 2006; 80(7):3567–3581. [PubMed: 16537625]

Daniels GM, Amara SG. Regulated trafficking of the human dopamine transporter. Clathrin-mediated internalization and lysosomal degradation in response to phorbol esters. J Biol Chem. 1999; 274(50):35794–35801. [PubMed: 10585462]

Delboy MG, Roller DG, Nicola AV. Cellular proteasome activity facilitates herpes simplex virus entry at a postpenetration step. J Virol. 2008; 82(7):3381–3390. [PubMed: 18234803]

Dey D, Shepherd A, Pachuau J, et al. Leukemia inhibitory factor regulates trafficking of T-type Ca2+ channels. Am J Physiol Cell Physiol. 2011; 300(3):C576–C587. [PubMed: 21178106]

Everett RD. ICP0, a regulator of herpes simplex virus during lytic and latent infection. BioEssays. 2000; 22(8):761–770. [PubMed: 10918307]

Figliozzi RW, Chen F, Balish M, Ajavon A, Hsia SV. Thyroid hormone-dependent epigenetic suppression of herpes simplex virus-1 gene expression and viral replication in differentiated neuroendocrine cells. J Neurol Sci. 2014; 346(1–2):164–173. [PubMed: 25175854]

Foster TP, Rybachuk GV, Kousoulas KG. Expression of the enhanced green fluorescent protein by herpes simplex virus type 1 (HSV-1) as an in vitro or in vivo marker for virus entry and replication. J Virol Methods. 1998; 75(2):151–160. [PubMed: 9870590]

Garber SS, Hoshi T, Aldrich RW. Regulation of ionic currents in pheochromocytoma cells by nerve growth factor and dexamethasone. J Neurosci. 1989; 9(11):3976–3987. [PubMed: 2479727]

Harley CA, Dasgupta A, Wilson DW. Characterization of herpes simplex virus-containing organelles by subcellular fractionation: role for organelle acidification in assembly of infectious particles. J Virol. 2001; 75(3):1236–1251. [PubMed: 11152497]

Hsia SC, Graham LP, Bedadala GR, et al. Induction of transcription factor early growth response protein 1 duringHSV-1 infection promotes viral replication in corneal cells. Br Microbiol Res J. 2013; 3(4):706–723. [PubMed: 25264522]

Hsia SC, Pinnoji RC, Bedadala GR, et al. Regulation of herpes simplex virus type 1 thymidine kinase gene expression by thyroid hormone receptor in cultured neuronal cells. J Neuro-Oncol. 2010; 16(1):13–24.

Iftinca MC, Zamponi GW. Regulation of neuronal T-type calcium channels. Trends Pharmacol Sci. 2009; 30(1):32–40. [PubMed: 19042038]

Kennedy PG, Montague P, Scott F, et al. Varicella-zoster viruses associated with post-herpetic neuralgia induce sodium current density increases in the ND7-23 Nav1.8 neuroblastoma cell line. PLoS One. 2013; 8:e51570. [PubMed: 23382806]

Kim JA, Park JY, Kang HW, et al. Augmentation of Cav3.2 T-type calcium channel activity by cAMP-dependent protein kinase A. J Pharmacol Exp Ther. 2006; 318(1):230–237. [PubMed: 16569752]

Krohel GB, Richardson JR, Farrell DF. Herpes simplex neuropathy. Neurology. 1976; 26(6):596–597. [PubMed: 945505]

Martin-Caraballo M, Greer JJ. Voltage-sensitive calcium currents and their role in regulating phrenic motoneuron electrical excitability during the perinatal period. J Neurobiol. 2001; 46(4):231–248. [PubMed: 11180152]

MeLean MJ, Bennett PB, Thomas RM. Subtypes of dorsal root ganglion neurons based on different inward currents as measured by whole-cell voltage clamp. Mol Cell Biochem. 1988; 80(1–2):95–107. [PubMed: 3173341]

Oakes SG, Petry RW, Ziegler RJ, et al. Electrophysiological changes of HSV-1-infected dorsal root ganglia neurons in culture. J Neuropathol Exp Neurol. 1981; 40(4):380–389. [PubMed: 6265604]

Pachuau J, Martin-Caraballo M. Extrinsic regulation of T-type Ca^{2+} channels in chick nodose ganglion cells. Dev Neurobiol. 2007; 67(14):1915–1931. [PubMed: 17874459]

Preston CM, Nicholl MJ. Repression of gene expression upon infection of cells with herpes simplex virus type 1 mutants impaired for immediate-early protein synthesis. J Virol. 1997; 71(10):7807–7813. [PubMed: 9311867]

Scott BS, Edwards BA. Electric membrane properties of adult mouse DRG neurons and the effect of culture duration. J Neurobiol. 1980; 11(3):291–301. [PubMed: 7391831]

Shah IM, Di Napoli M. The ubiquitin-proteasome system and proteasome inhibitors in central nervous system diseases. Cardiovasc Hematol Disord Drug Targets. 2007; 7(4):250–273. [PubMed: 18220725]

Storey N, Latchman D, Bevan S. Selective internalization of sodium channels in rat dorsal root ganglion neurons infected with herpes simplex virus-1. J Cell Biol. 2002; 158(7):1251–1262. [PubMed: 12356869]

Takasaki I, Andoh T, Shiraki K, et al. Allodynia and hyperalgesia induced by herpes simplex virus type-1 infection in mice. Pain. 2000; 86(1–2):95–101. [PubMed: 10779666]

Todorovic SM, Jevtovic-Todorovic V. T-type voltage-gated calcium channels as targets for the development of novel pain therapies. Br J Pharmacol. 2011; 163(3):484–495. [PubMed: 21306582]

Umemiya M, Berger AJ. Properties and function of low- and high-voltage-activated Ca2+ channels in hypoglossal motoneurons. J Neurosci. 1994; 14(9):5652–5660. [PubMed: 8083761]

van Loo KM, Schaub C, Pernhorst K, et al. Transcriptional regulation of T-type calcium channel CaV3.2: bi-directionality by early growth response 1 (Egr1) and repressor element 1 (RE-1) protein-silencing transcription factor (REST). J Biol Chem. 2012; 287(19):15489–15501. [PubMed: 22431737]

Weinheimer SP, McKnight SL. Transcriptional and posttranscriptional controls establish the cascade of herpes simplex virus protein synthesis. J Mol Biol. 1987; 195(4):819–833. [PubMed: 2821283]

Wittels M, Spear PG. Penetration of cells by herpes simplex virus does not require a low pH-dependent endocytic pathway. Virus Res. 1991; 18(2–3):271–290. [PubMed: 1645908]

Wood JN, Bevan SJ, Coote PR, et al. Novel cell lines display properties of nociceptive sensory neurons. Proc Biol Sci. 1990; 241(1302):187–194. [PubMed: 1979443]

Woodall AJ, Richards MA, Turner DJ, et al. Growth factors differentially regulate neuronal Cav channels via ERK-dependent signalling. Cell Calcium. 2008; 43(6):562–575. [PubMed: 17996937]

Yin K, Baillie GJ, Vetter I. Neuronal cell lines as model dorsal root ganglion neurons: a transcriptomic comparison. Mol Pain. 2016; 12:1–17.

Zhou Y, Frey TK, Yang JJ. Viral calciomics: interplays between Ca2+ and virus. Cell Calcium. 2009; 46(1):1–17. [PubMed: 19535138]

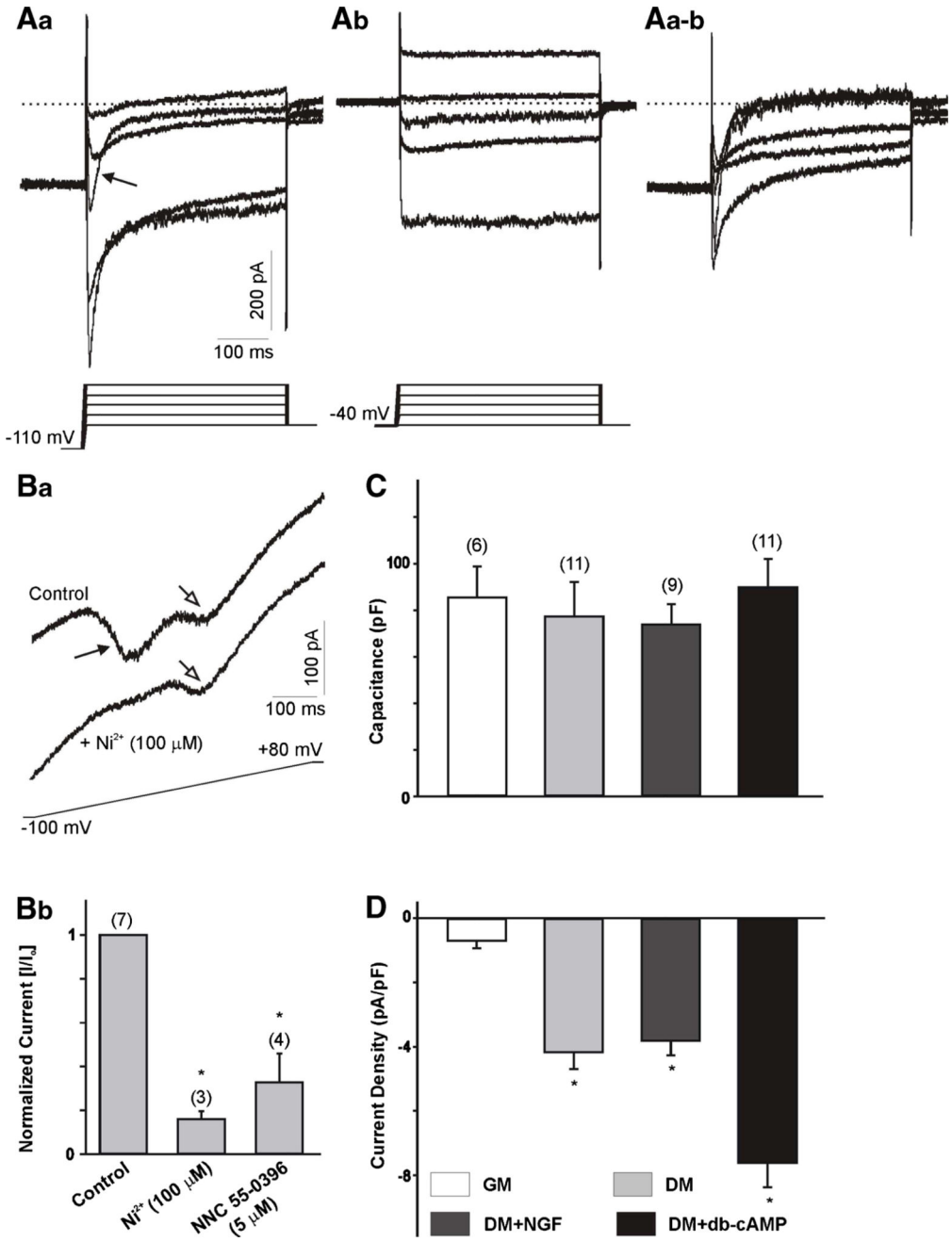

Fig. 1.

Whole cell Ca^{2+} currents in ND7-23 cells. *Aa–b* Example of whole cell Ca^{2+} currents generated in a differentiated ND7-23 cell. Current traces obtained from a holding potential of −110 mV (*Aa*) or from a holding potential of −40 mV (*Ab*). In this and subsequent figures, the voltage step protocol is shown below the current trace. Note that the transient component (*arrow*) generated by voltage steps from a holding potential of −110 mV was eliminated when the currents were generated from a holding potential of −40 mV. *Aa–b* Digital subtraction of *Aa* and *Ab* traces shows the inactivating component and represents the LVA (or T-type) Ca^{2+} currents used for further studies. *B* Example of whole cell Ca^{2+}

currents generated in a differentiated ND7-23 cell by a voltage ramp before and after the application of 100 μM $NiCl_2$. Note the two peaks generated by the activation of LVA and HVA Ca^{2+} channels (*Ba*). Only the peak current generated by activation of LVA Ca^{2+} channels was sensitive to blockade with $NiCl_2$. *Bb* Treatment of differentiated ND7-23 cells with $NiCl_2$ or NNC 55–0396 causes a significant reduction in the peak current generated by activation of LVA Ca^{2+} channels. In this and subsequent figures, *error bars* represent SEM and the number of cells recorded is provided above each bar. The *asterisk* denotes $p < 0.05$ vs. control. *C* Comparison of cell capacitance in ND7-23 cells before and after induction of cell differentiation with differentiation media supplemented with NGF or db-cAMP. ND7-23 cells were cultured for ~10 days with growth media (GM) or differentiation media (DM) supplemented with NGF (50 ng/mL) or db-cAMP (1 mM). *D* Mean T-type Ca^{2+} current densities generated in ND7-23 cells under different culture conditions. Note the robust stimulation of T-type Ca^{2+} current densities in ND7-23 cells cultured in differentiation media with or without NGF or db-cAMP. T-type Ca^{2+} current density was calculated from the peak current amplitude generated by a voltage step to −20 mV from the digital subtraction of current traces at −110 and −40 mV. The *asterisk* denotes $p < 0.05$ vs. growth media (GM)

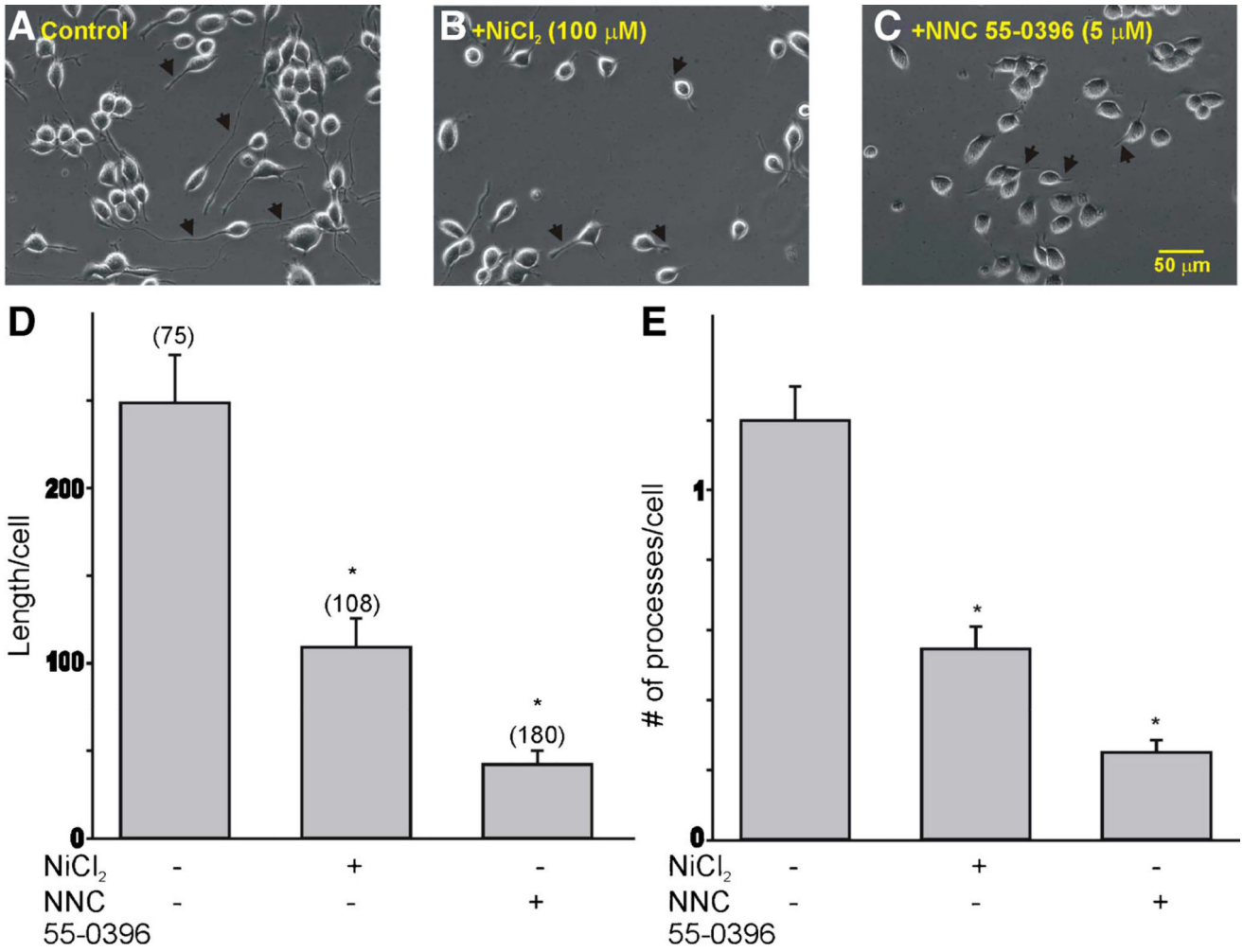

Fig. 2.

T-type Ca^{2+} channel expression regulates the neurite-like morphology of differentiated ND7-23 cells. **a–c** Phase contrast images of differentiated ND7-23 cells before and after treatment with the T-type Ca^{2+} channel blockers $NiCl_2$ (100 μM) or NNC 55-0396 (5 μM). *Arrows* point to differences in neurite length between control and Ni^{2+} ions or NNC 55-0396-treated cells. Note that Ni^{2+} ions and NNC 55-0396 evoke a significant decrease in the neurite-like outgrowth and morphology of differentiated ND7-23 cells compared to non-treated controls. **d, e** Summary of changes in the length and number of neurite-like processes/cell in differentiated ND7-23 cells following inhibition of T-type Ca^{2+} channel function with $NiCl_2$ (100 μM) or NNC 55–0396 (5 μM) (*$p < 0.05$ vs. control)

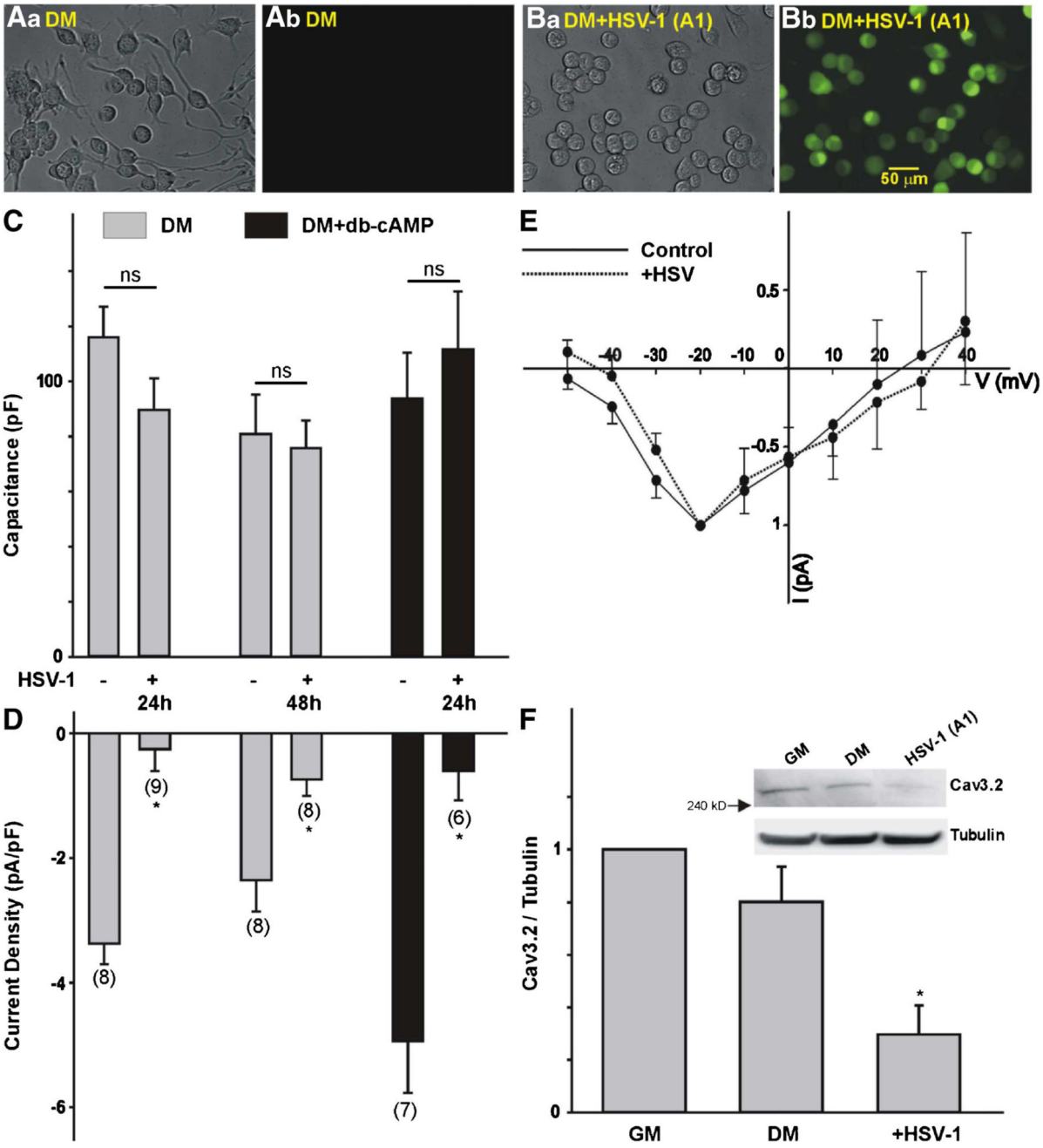

Fig. 3.

Effect of HSV-1 infection on T-type Ca^{2+} channel expression in differentiated ND7-23 cells. *A, B* Phase contrast (*Aa, Ba*) and GFP fluorescence (*Ab, Bb*) images of differentiated ND7-23 cells following HSV-1 infection. Differentiated ND7-23 cells express GFP fluorescence following overnight infection with HSV-1 (*Bb*) but not in non-infected cells (*Ab*). *C* Comparison of cell capacitance in ND7-23 cells before and after HSV-1 infection. Note that infection of differentiated ND7-23 cells had no effect on cell capacitance. ND7-23 cells were cultured for ~10 days with differentiation media (DM) alone or supplemented with db-cAMP (1 mM). After induction of cell differentiation, cells were infected with

HSV-1 for 1 h. After this time period, viral particles were removed by washing with fresh media and cells were maintained for up to 48 h before performing whole cell recording of Ca^{2+} currents. *D* Infection of differentiated ND7-23 cells with HSV-1 causes a significant reduction in T-type Ca^{2+} current densities under all conditions tested. *E* Current-voltage (I–V) relationship for the peak current amplitude generated by a voltage step to −20 mV in ND7-23 cells before and after infection with HSV-1 for 24 h. *F* Changes in the expression of the $Ca_v3.2$ T-type Ca^{2+} channel subunit as determined by densitometry analysis (*$p < 0.05$ vs. non-infected cells grown in differentiation media (DM), $n = 5$). *Inset*: Representative example of western blot data collected from ND7-23 cells following infection with HSV-1. To confirm equal loading, membranes were stripped following $Ca_v3.2$ immunoblot and reprobed for tubulin. The ratio of $Ca_v3.2$ to tubulin was used to assess changes in $Ca_v3.2$ expression by densitometry analysis

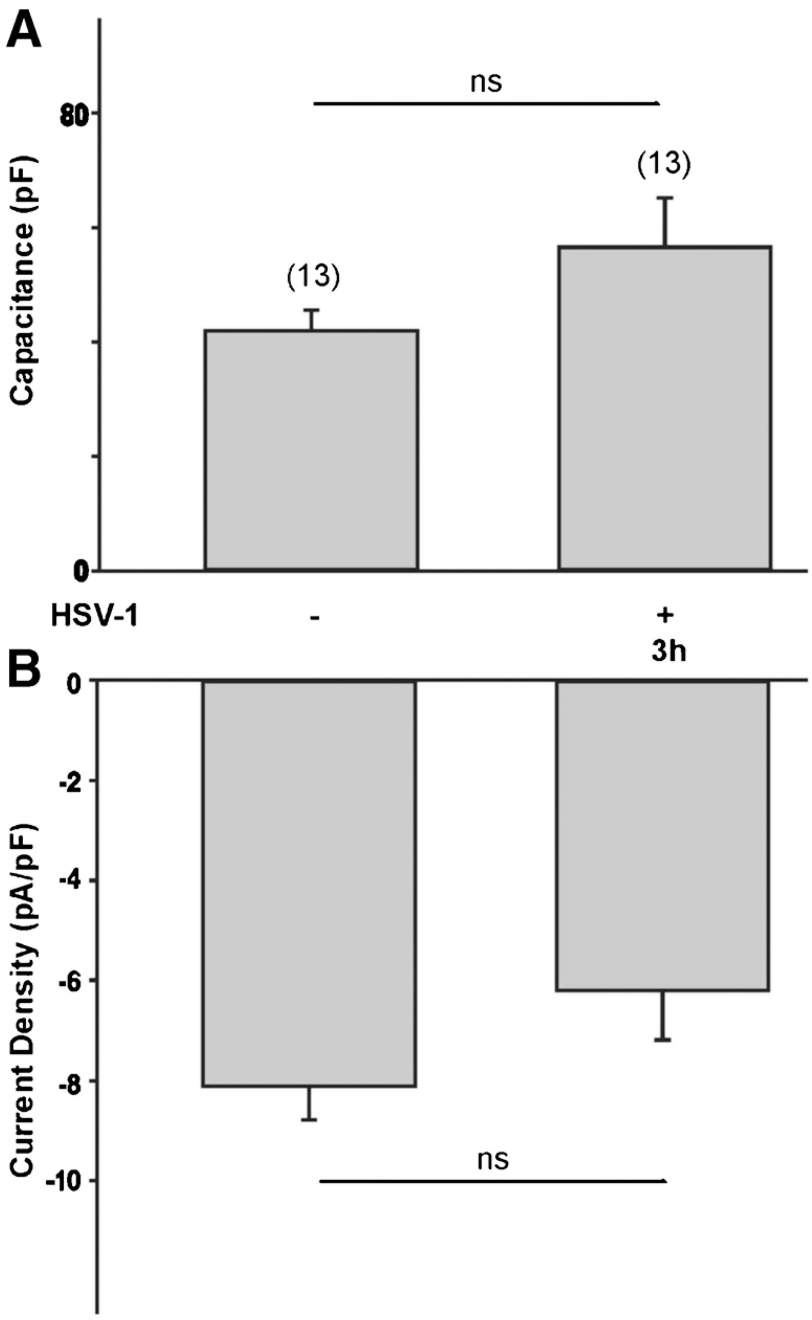

Fig. 4.

Effect of short term viral infection on T-type Ca^{2+} channel expression in differentiated ND7-23 cells. **a, b** A 3 h viral infection with HSV-1 did not have any significant effect on the cell capacitance and T-type Ca^{2+} current density of differentiated ND7-23 cells. ND7-23 cells were cultured for ~4 days with differentiation media (DM) supplemented with NGF (50 ng/mL) + db-cAMP (1 mM). After cell differentiation, cells were infected for 1 h with HSV-1 (moi=5). After this time period, viral particles were removed by washing with fresh media and cells were maintained for up to 3 h before performing whole cell recording of Ca^{2+} currents

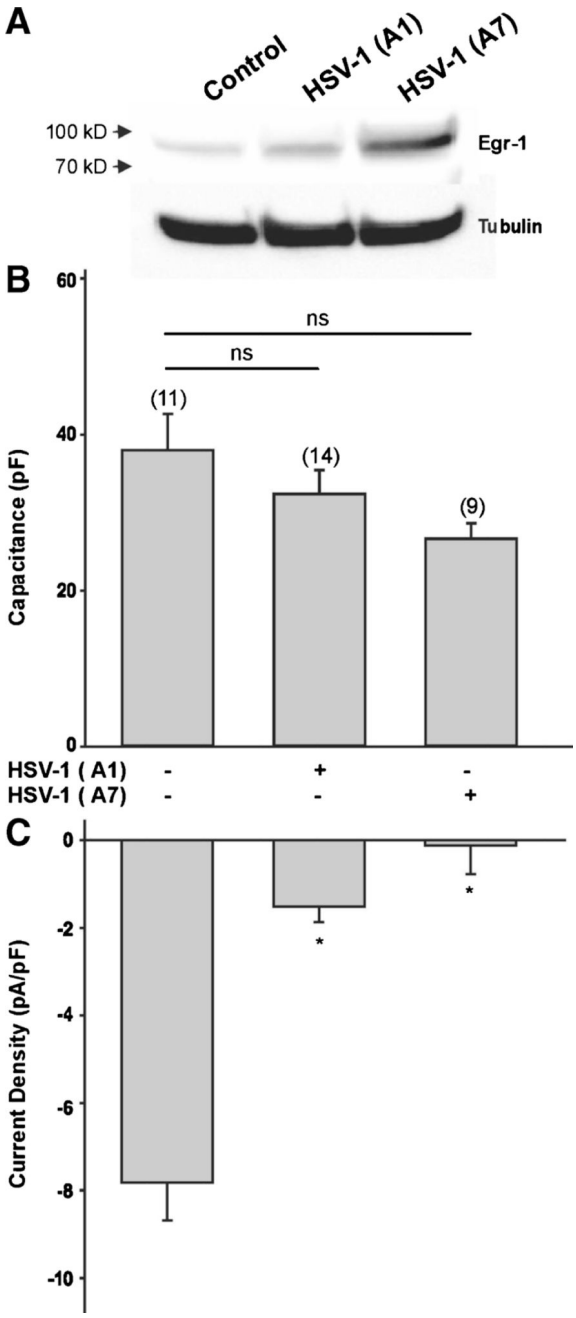

Fig. 5.

Effect of Egr-1 on T-type Ca^{2+} channel expression in differentiated ND7-23 cells. **a** Western blot analysis comparing the expression levels of Egr-1 protein in differentiated ND7-23 cells following infection with the HSV-1 viral strains A1 and A7. **b, c** Viral infection with HSV-1 A1 and A7 strain did not have any significant effect on the cell capacitance of differentiated ND7-23 cells. However, HSV-1 A1 and A7 infections caused a significant reduction in T-type Ca^{2+} current density. ND7-23 cells were cultured for ~4 days with differentiation media (DM) supplemented with NGF (50 ng/mL) + db-cAMP (1 mM). After induction of cell differentiation, cells were infected for 1 h with HSV-1 A1 or A7 strains. After this time

period, viral particles were removed by washing with fresh media and cells were maintained for up to 24 h before performing whole cell recording of Ca^{2+} currents

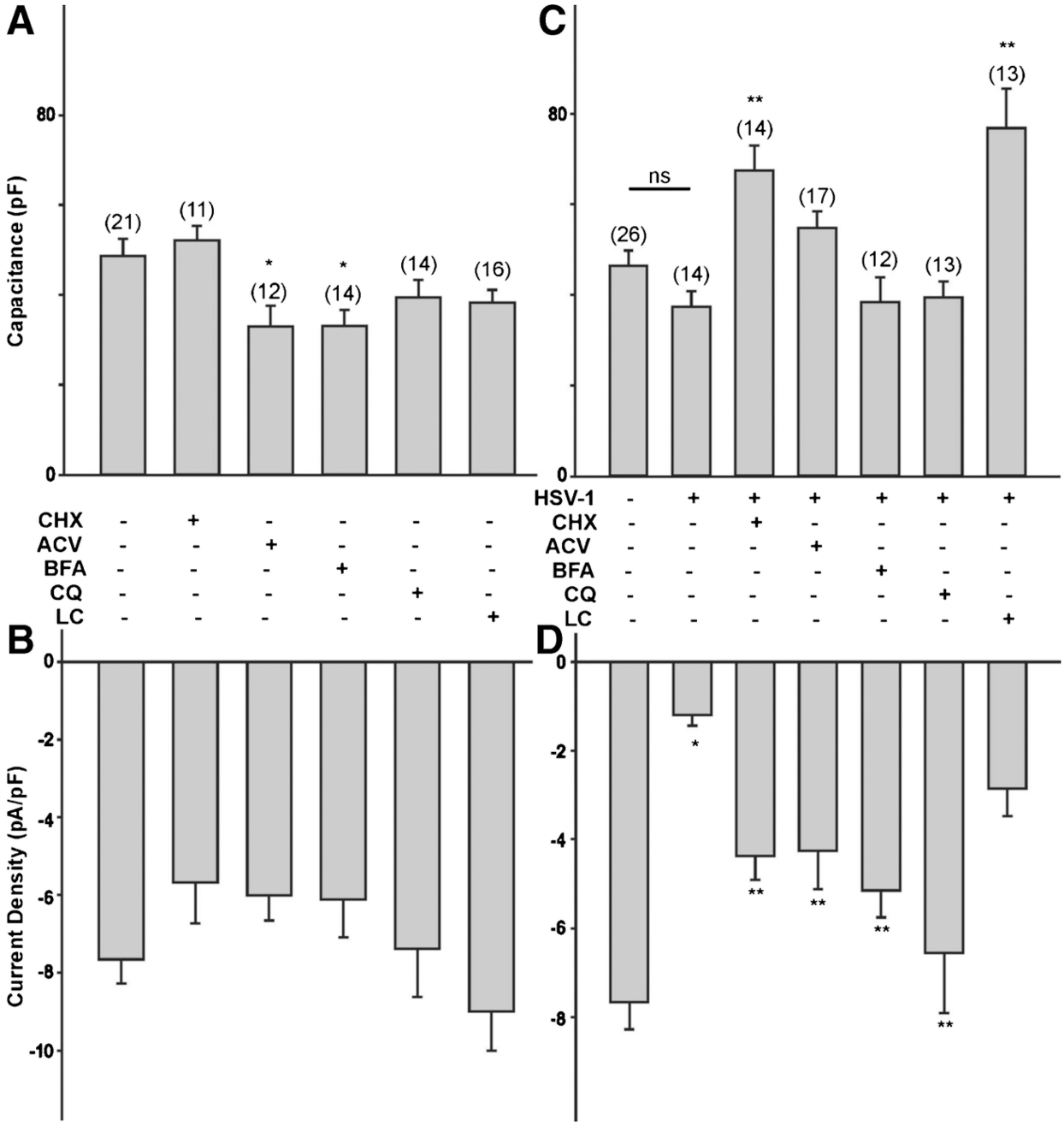

Fig. 6.

Effect of cycloheximide, acyclovir, brefeldin-A, chloroquine, and lactacystin on T-type Ca^{2+} channel expression following infection of differentiated ND7-23 cells with HSV-1. ND7-23 cells were cultured for ~4 days with differentiation media, supplemented with NGF (50 ng/mL) + db-cAMP (1 mM). After induction of cell differentiation, cells were infected with HSV-1 for 1 h to allow viral binding and penetration. After this time period, viral particles were removed by washing with fresh media (containing specific inhibitors) and cells were maintained overnight before performing whole cell recording of Ca^{2+} currents. **a, b** Effect of cycloheximide, acyclovir, brefeldin-A, chloroquine, and lactacystin on cell capacitance and

T-type Ca^{2+} current density on differentiated ND7-23 cells. Note that only acyclovir and brefeldin-A cause a significant reduction in the cell capacitance of differentiated ND7-23. All the drugs tested have no overall effect on T-type Ca^{2+} current density. **c, d** Effect of cycloheximide, acyclovir, brefeldin-A, chloroquine, and lactacystin on the cell capacitance and T-type Ca^{2+} current density of differentiated ND7-23 cells following HSV-1 infection. Note that HSV-1 infection causes a considerable reduction in T-type Ca^{2+} current density compared with non-infected cells (the *asterisk* denotes $p < 0.05$ vs. non-infected cells). HSV-1 infection has no effect on cell capacitance. Inhibition of protein synthesis and viral replication with cycloheximide and acyclovir, respectively, causes a significant increase in the T-type Ca^{2+} current density of cells infected with HSV-1 (the *double asterisk* denotes $p < 0.05$ vs. HSV-1-infected cells). Similarly, treatment with brefeldin-A and chloroquine, but not lactacystin, reverses the inhibitory effect of HSV-1 infection on T-type Ca^{2+} current density. Cycloheximide and lactacystin also evoke a considerable increase in the cell capacitance of ND7-23 cells infected with HSV-1 (the *double asterisk* denotes $p < 0.05$ vs. HSV-1-infected cells)

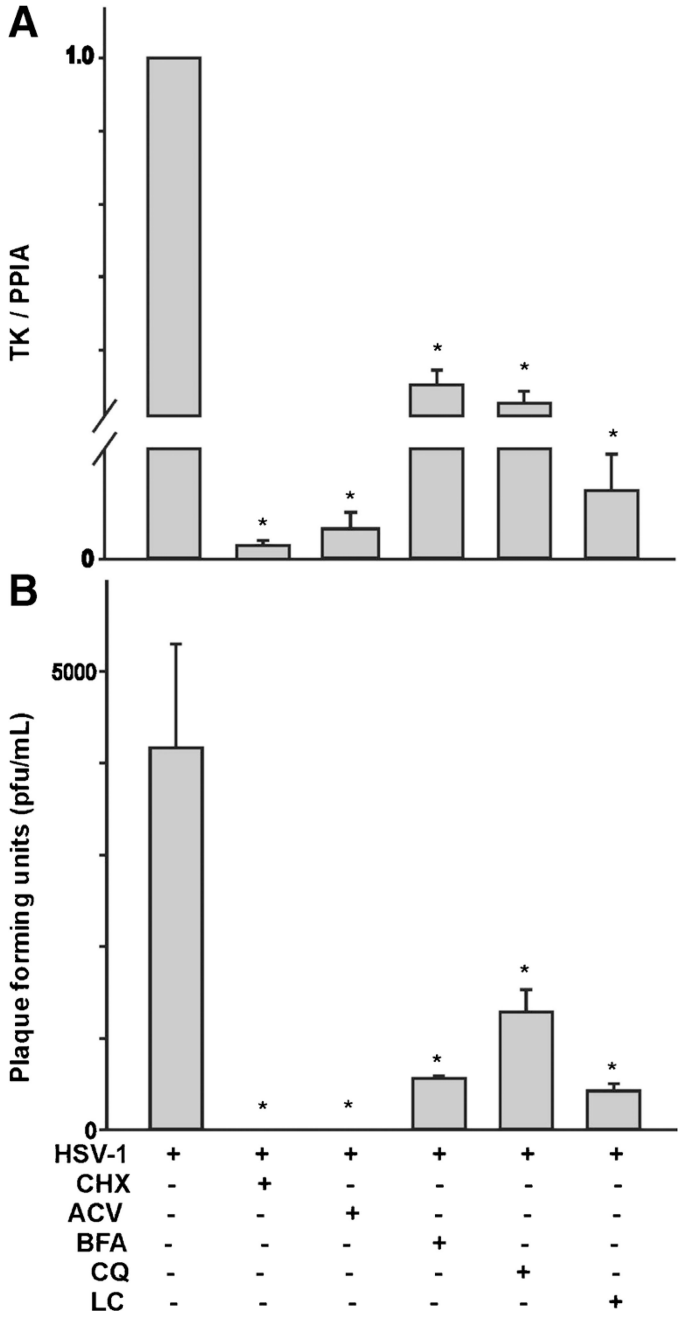

Fig. 7.

Effect of cycloheximide, acyclovir, brefeldin-A, chloroquine, and lactacystin on viral replication following infection of differentiated ND7-23 cells with HSV-1. **a** Cycloheximide, acyclovir, brefeldin-A, chloroquine, and lactacystin evoke a considerable reduction in the expression of the HSV-1 TK (the *asterisk* denotes $p < 0.05$ vs. HSV-1-infected cells, n=4). **b** Cycloheximide, acyclovir, brefeldin-A, chloroquine, and lactacystin cause a significant decrease in plaque formation (the *asterisk* denotes $p < 0.05$ vs. HSV-1-infected cells, n=4)

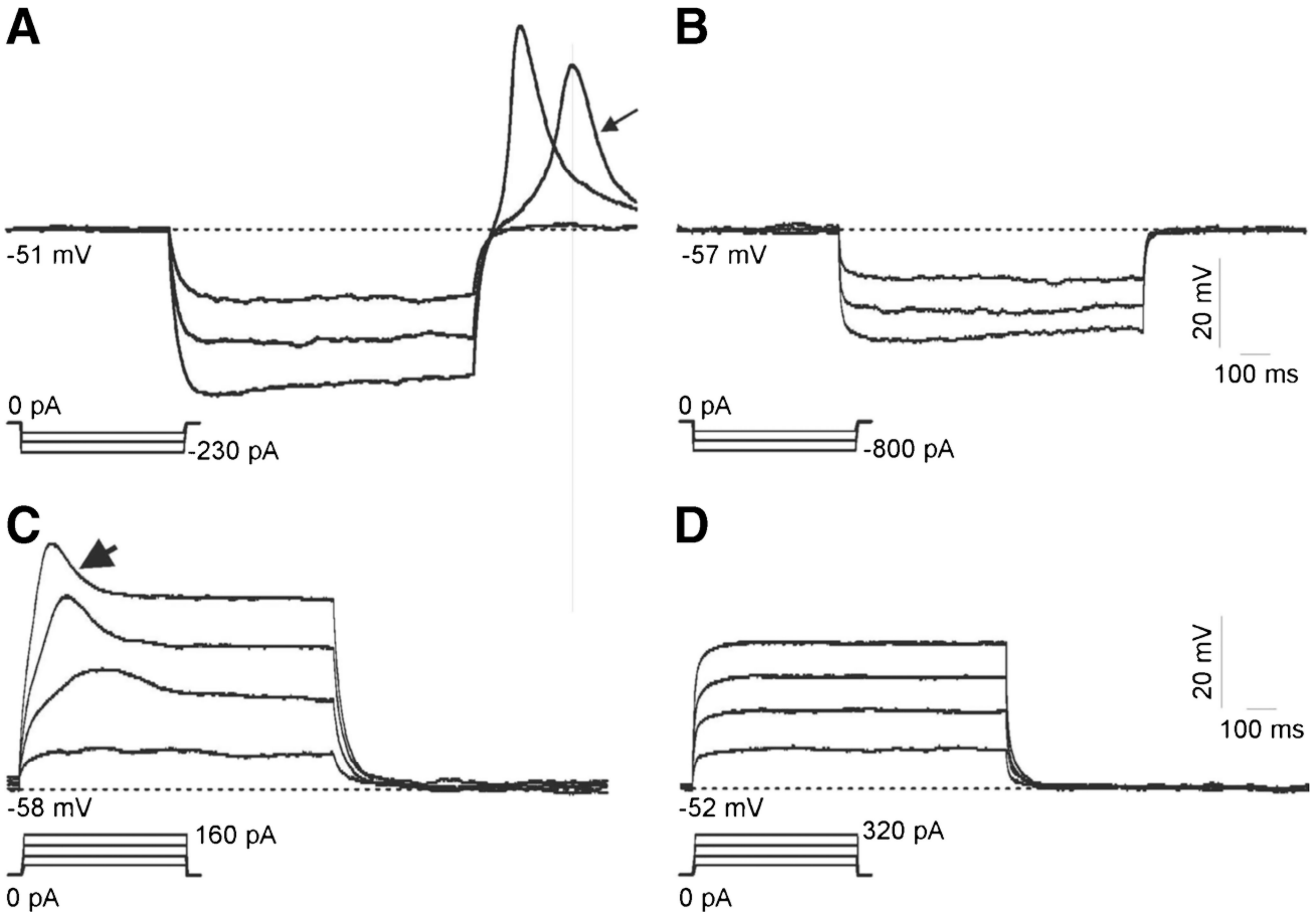

Fig. 8.

Effect of HSV-1 infection on the rebound depolarization of differentiated ND7-23 cells. **a, b** Differentiated ND7-23 cells express a prominent rebound depolarization (*arrow* in **A**) following injection of hyperpolarizing current. Infection of differentiated ND7-23 cells with HSV-1 eliminates the expression of rebound depolarization (**b**). The presence of rebound depolarization was assessed in the current clamp configuration following the injection of negative current (see current protocol shown below voltage responses in **a** and **b**). **c, d** Recording of voltage responses to injection of depolarizing currents demonstrated the lack of Na^+-dependent spikes. Current injection protocol is shown below voltage responses in **c** and **d**. In non-infected cells, injection of depolarizing currents evokes a spikelet (*arrowhead* in **c**). ND7-23 cells were cultured for ~4 days with differentiation media (DM) supplemented with NGF (50 ng/mL) + db-cAMP (1 mM). After induction of cell differentiation, cells were infected for 1 h with HSV-1. After this time period, viral particles were removed by washing with fresh media and cells were maintained overnight before performing current clamp recordings

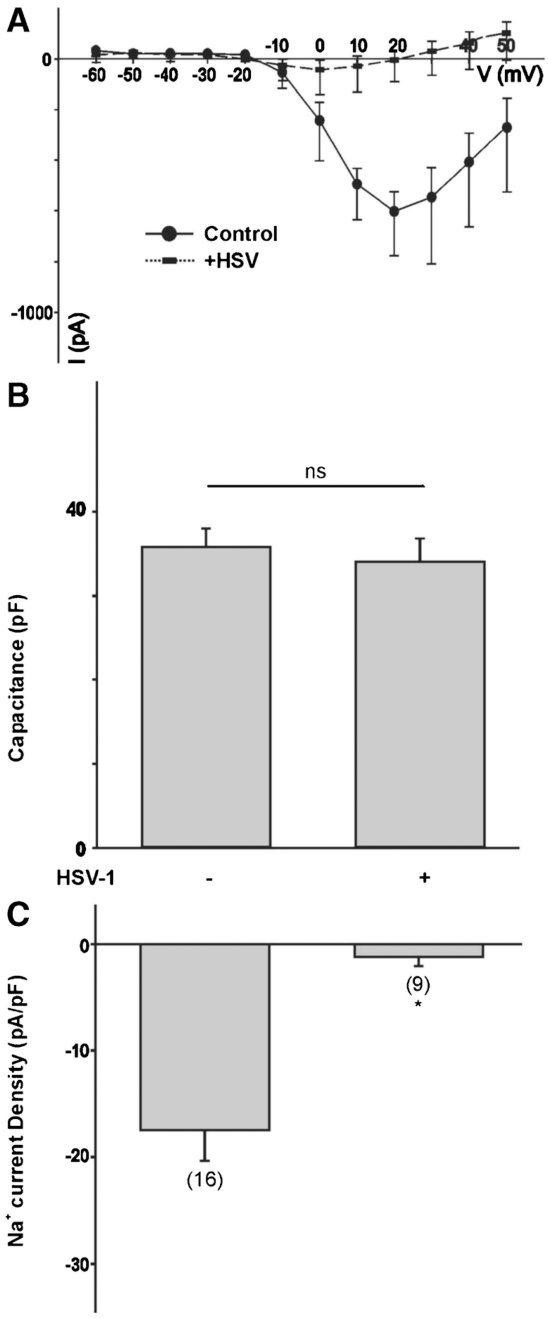

Fig. 9.

Effect of HSV-1 infection on Na^+ channel expression in differentiated ND7-23 cells. **a** Current-voltage (I–V) relationship for the peak Na^+ current amplitude generated by a series of voltage steps from a holding potential of −100 mV in ND7-23 cells before and after infection with HSV-1 for 24 h. **b** Comparison of cell capacitance in ND7-23 cells before and after HSV-1 infection. ND7-23 cells were cultured for ~4–7 days with differentiation media (DM) alone or supplemented with db-cAMP (1mM) + NGF (50 ng/mL). After induction of cell differentiation, cells were infected with HSV-1 for 1 h. **c** Infection of differentiated

ND7-23 cells with HSV-1 causes a significant reduction in the density of Na^+ currents under all conditions tested (the *asterisk* denotes $p < 0.05$ vs. HSV-1-infected cells)